



1 **Moist moss tundra on Kapp Linne, Svalbard is a net source of CO<sub>2</sub> and CH<sub>4</sub> to the**  
2 **atmosphere**

3 **Anders Lindroth<sup>1</sup>, Norbert Pirk<sup>2</sup>, Ingibjörg S Jónsdóttir<sup>3</sup>, Christian Stiegler<sup>4</sup>, Leif**  
4 **Klemedtsson<sup>5</sup>, and Mats B Nilsson<sup>6</sup>**

5 <sup>1</sup>Department of Physical Geography and Ecosystem Science, Lund University, Lund, Sweden.

6 <sup>2</sup>Department of Geosciences, University of Oslo, Oslo, Norway.

7 <sup>3</sup>Life and Environmental Sciences, University of Iceland, Reykjavik, Iceland.

8 <sup>4</sup>Bioclimatology, Georg-August Universität Göttingen, Göttingen, Germany.

9 <sup>5</sup>Department of Earth Sciences, University of Gothenburg, Gothenburg, Sweden.

10 <sup>6</sup>Department of Forest Ecology and Management, Swedish University of Agricultural Sciences,  
11 Umeå, Sweden.

12 Corresponding author: anders.lindroth@nateko.lu.se



## 13 Abstract

14 We measured CO<sub>2</sub> and CH<sub>4</sub> fluxes using chambers and eddy covariance (only CO<sub>2</sub>) from a moist  
15 moss tundra in Svalbard. The average net ecosystem exchange (NEE) during the summer (June-  
16 August) was -0.40 g C m<sup>-2</sup> day<sup>-1</sup> or -37 g C m<sup>-2</sup> for the whole summer. Including spring and  
17 autumn periods the NEE was reduced to -6.8 g C m<sup>-2</sup> and the annual NEE became positive, 24.7  
18 g C m<sup>-2</sup> due to the losses during the winter. The CH<sub>4</sub> flux during the summer period showed a  
19 large spatial and temporal variability. The mean value of all 214 samples was  
20 0.000511±0.000315 μmol m<sup>-2</sup>s<sup>-1</sup> which corresponds to a growing season estimate of 0.04 to 0.16  
21 g CH<sub>4</sub> m<sup>-2</sup>. We find that this moss tundra emits about 94-100 g CO<sub>2</sub>-equivalents m<sup>-2</sup> yr<sup>-1</sup> of which  
22 CH<sub>4</sub> is responsible for 3.5-9.3% using GWP<sub>100</sub> of 27.9 respectively GWP<sub>20</sub>.

23  
24 Air temperature, soil moisture and greenness index contributed significantly to explain the  
25 variation in ecosystem respiration (R<sub>eco</sub>) while active layer depth, soil moisture and greenness  
26 index were the variables that best explained CH<sub>4</sub> emissions. Estimate of temperature sensitivity  
27 of R<sub>eco</sub> and gross primary productivity showed that a modest increase in air temperature of 1  
28 degree did not significantly change the NEE during the growing season but that the annual NEE  
29 would be even more positive adding another 8.5 g C m<sup>-2</sup> to the atmosphere. We tentatively  
30 suggest that the warming of the Arctic that has already taken place is partly responsible for the  
31 fact that the moist moss tundra now is a source of CO<sub>2</sub> to the atmosphere.

## 32 1 Introduction

33 Climate warming is predicted to be most evident at high latitudes (Friedlingstein et al., 2006)  
34 with profound effects on ecosystem functioning. One of the high latitude regions that are  
35 expected to experience the most dramatic changes caused by climate change is the Arctic. This  
36 region which is located roughly north of the tree-line is characterized by cold winters and cool  
37 summers and with mean annual temperatures below zero. The summer periods are short ranging  
38 between 3.5 to 1.5 months from the southern boundary to the north and July is normally the  
39 warmest month. Annual precipitation is generally low decreasing from about 250 mm in the  
40 southern areas to 45 mm in polar deserts in the north (Callaghan et al., 2005).

41  
42 The permafrost soils in the Arctic store 1035±150 Pg of organic carbon in the top 0-3 m  
43 (Hugelius et al., 2014) which is more than the average 2010-2019 of 860 Pg of carbon in the  
44 atmosphere (Friedlingstein et al., 2020). The increased warming in these areas can induce higher  
45 decomposition rates due to increased microbial activity which will provide a positive feedback to  
46 the climate system (Schuur et al., 2015). On the other hand, warming can also increase  
47 photosynthesis and carbon uptake and thus compensate for, or exceed, the effect of increased  
48 decomposition. Climate warming is also affecting plant community composition and the length  
49 of the growing season (Post et al., 2009) which also has an impact on the processes regulating  
50 annual carbon emissions and uptake (Bosiö et al., 2014). There is however a large uncertainty  
51 regarding the timing, magnitude and possible sign of potential feedbacks caused by these  
52 changes (Myers-Smith et al., 2020).

53  
54 Understanding processes that are controlling the exchanges of greenhouse gases in the Arctic is  
55 crucial for assessment of potential feedback effects. For this purpose, multiple year-around long-  
56 term studies including direct measurements of CO<sub>2</sub> and CH<sub>4</sub> fluxes covering all seasons, winter,  
57 spring, summer and autumn would be ideal. This is a great challenge in the harsh climate of the



58 Arctic and with limited support of key infrastructures for, e.g., provision of electricity for  
59 operation of instruments.

60

61 In spite of these difficulties a few year-around studies have been performed during the last  
62 couple of decades. In the low Arctic, Oechel et al. (2013) demonstrate the importance of the  
63 wintertime fluxes in a tussock tundra ecosystem in Alaska. They found that the non-summer  
64 season emitted more CO<sub>2</sub> than the corresponding uptake during the summer resulting in a net  
65 source to the atmosphere of about 14 g C m<sup>-2</sup> on an annual basis. They also showed that the  
66 shoulder seasons, spring and autumn roughly out-weighted the summer uptake. Euskirchen et al.  
67 (2012, 2016) measured net CO<sub>2</sub> exchange in three different tundra ecosystems; heath tundra,  
68 tussock tundra and wet sedge tundra in northern Alaska over three years. They found that the  
69 uptake of -51 to -95 g C m<sup>-2</sup> during the summer (June-August) was overturned by the respiration  
70 that occurred during the winter period resulting in net annual losses for all three ecosystems.  
71 Zhang et al. (2019) reported five years of year-around flux measurements in a heath ecosystem  
72 on west Greenland and they found that the heath was an annual sink of -35±15 g C m<sup>-2</sup>. One year  
73 with an anomalously deep snow pack showed a 3-fold higher respiration during the winter as  
74 compared to the other years which resulted in a significantly lower net uptake during that year.

75

76 Even fewer studies have been done on year-around studies in the high Arctic. Lüers et al. (2014)  
77 quantified the annual CO<sub>2</sub> budget using eddy covariance measurements in a river catchment area  
78 near Ny-Ålesund on Spitsbergen in the Svalbard archipelago and they found that the ecosystem  
79 was in C-balance. The footprint area was a semi-polar desert with only 60% vegetation cover and  
80 patches of bare soil and stones. Also in Svalbard but further south in Adventdalen on a flat  
81 alluvial fen irregularly covered with ice wedged polygons, Pirk et al. (2017) made year-around  
82 measurements of CO<sub>2</sub> fluxes and found it to be a net sink of -82 g C m<sup>-2</sup>. Because of the  
83 irregularities caused by the ice wedges and the differences in wetness, they focused the analyses  
84 on the spatial variability in two different directions, one wetter and one drier, and they estimated  
85 the annual net ecosystem exchange to -91 g C m<sup>-2</sup> and -62 g C m<sup>-2</sup> for the respective areas.

86

87 The Arctic ecosystems constitute also a source of CH<sub>4</sub> to the atmosphere even if it is not a very  
88 large one. Saunio et al. (2020) estimated that the Northern high latitude region (60°N - 90°N)  
89 contributed 4% of global emissions and emissions from wetlands are only part of the emissions  
90 from this region. However, in the light of the vulnerability of the high Arctic permafrost areas  
91 and considering the large carbon pool and the predicted changes in climate, a quantification and  
92 understanding of CH<sub>4</sub> exchanges in these areas are still important. Christensen et al. (2004)  
93 showed one example of a dramatic impact of the climate warming on the CH<sub>4</sub> emissions in a  
94 permafrost mire in sub-arctic Sweden. The warming which is visible in this area since decades  
95 and its impact on permafrost and vegetation changes was estimated to have caused an increase of  
96 landscape CH<sub>4</sub> emissions in the range 22-66% in the period 1970 to 2000.

97

98 Mastepanov et al. (2008) were the first to show the importance of emissions also outside of the  
99 growing season. They observed a large burst of CH<sub>4</sub> from a fen area in Zackenberg, Greenland  
100 after the growing season and during the time when the soil started to freeze. This finding was  
101 confirmed in a later paper (Mastepanov et al., 2013) and the process was hypothetically  
102 attributed to the subsurface CH<sub>4</sub> pool. Hydrology and vegetation composition play an important  
103 role for CH<sub>4</sub> emission and dynamics. McGuire et al. (2012) made a comprehensive summary of



104 CH<sub>4</sub> exchanges of the Arctic tundra showing the difference between wet and dry ecosystems; the  
105 wet tundra emitted 5.4 to 13.0 g CH<sub>4</sub>-C m<sup>-2</sup> during summer and 8.5 to 20.2 g CH<sub>4</sub>-C m<sup>-2</sup>  
106 annually. The corresponding values for the dry/mesic tundra were 0.3 to 1.4 g CH<sub>4</sub>-C m<sup>-2</sup> and 0.3  
107 to 4.3 g CH<sub>4</sub>-C m<sup>-2</sup>, respectively. Bao et al. (2021) utilized year-around measurements of CH<sub>4</sub>  
108 fluxes from three sites of the Ameriflux network in Northern Alaska to demonstrate the  
109 importance of the spring and autumn seasons for the annual emission. The shoulder seasons  
110 contributed about 25% of the annual emissions and the autumn season had about three times  
111 higher emission than the spring season. These findings increasingly emphasise the importance of  
112 year-around measurements to fully understand the CH<sub>4</sub> controls and dynamics.  
113

114 The main aim of this study is to provide another piece of the puzzle concerning CO<sub>2</sub> and CH<sub>4</sub>  
115 exchanges from different but widespread ecosystem types in the high Arctic. We hypothesise  
116 that this moist tundra ecosystem is a net annual carbon sink and that the summer emissions of  
117 methane will be at average levels. We made flux measurements of CO<sub>2</sub> and CH<sub>4</sub> in an moist  
118 moss tundra ecosystem situated at Kapp Linne on the west coast of the Svalbard archipelago in  
119 2015 and with an additional campaign in 2016. The measurements in 2015 were done using both  
120 eddy covariance system (CO<sub>2</sub>) and chambers (CO<sub>2</sub> and CH<sub>4</sub>) but only chambers in 2016. We  
121 quantify ecosystem respiration (R<sub>eco</sub>), gross primary productivity (GPP) and net ecosystem  
122 exchange (NEE) during the growing season based on measurements and we extend the time  
123 period to a full year by modelling. The CH<sub>4</sub> emission was only quantified for the summer season.  
124 We also analyze the environmental controls of the fluxes.

## 125 **2 Materials and Methods**

### 126 **2.1 Research site and measurements**

127  
128 This study was performed in the Svalbard archipelago near the weather station Isfjord Radio  
129 (78°03'08" N 13°36'04" E, alt. 7 m) which is located right on the foreland of Kapp Linné on the  
130 island of Spitzbergen (Fig. S1). The tundra area where the measurements were performed is  
131 located about 1 km southeast of the station. The study area consists of moist moss tundra, a  
132 widespread ecosystem in Svalbard (Vanderpuyé et al., 2002; Ravolainen et al., 2020). The  
133 vegetation is characterised by the moss species *Tomentypnum nitens*, *Sanionia uncinata* and  
134 *Aulacomium palustre* and a sparse cover of vascular plants (20-40%), dominated by *Equisetum*  
135 *arvense*, *Salix polaris* and *Bistorta vivipara*. Other vascular plant species found in the plots:  
136 *Saxifraga cespitosa*, *Saxifraga oppositifolia*, *Silene aucaulis*, and some grass species, most likely  
137 *Alopecurus ovatus* (previously *A. borealis*), and *Poa arctica*. The vegetation analysis was made  
138 from photographs of chamber location plots taken between 26 June and 2 July 2015 (see Figs.  
139 S4a-4y in Supplement).  
140

141 The net ecosystem exchange of CO<sub>2</sub> was measured with an eddy covariance (EC) system located  
142 centrally on the moss tundra (78°03'28.6" N 13°38'40" E). The sonic anemometer (USA-1;  
143 Metek GmbH, Germany) was mounted on top of a tripod (see Fig. S1) at 2.7 m height. The CO<sub>2</sub>  
144 and H<sub>2</sub>O concentrations were measured with an open path sensor (LI-7500; Li-Cor Inc., USA)  
145 placed just beneath the sonic and inclined about 30° pointing towards east. Radiation  
146 components, incoming and outgoing short-wave and long-wave (CNR-4; Kipp & Zonen, the  
147 Netherlands) were measured at 2.0 m height above ground with the sensor directed towards



148 south. All sensors were connected to a datalogger (CR-1000; Campbell Scientific, USA) which  
149 was powered by a solar panel and a battery. The EC sensors were sampled and stored at 10 Hz  
150 and all other sensors were sampled at 0.1 Hz with storage of 30 min mean values. These  
151 measurements were made from 25 June to 17 September 2015.

152

153 The soil efflux of CO<sub>2</sub> and CH<sub>4</sub> was measured with a dark chamber connected to a gas analyzer  
154 (Ultraportable Greenhouse Gas Analyzer; Los Gatos Research, USA) on 24 locations within the  
155 EC average footprint area. A circular thin-steel frame, 15 cm in diameter and 15 cm high, was  
156 inserted ca 5 cm into the ground in each location. The sharp edge of the frames made it easy to  
157 insert them into the ground without damaging the vegetation and with minimal soil disturbance.  
158 A picture was taken of each frame (see Supplement) for documentation of vegetation and for  
159 calculation of different indexes. The chamber was also made from steel and it had a rubber seal  
160 in the end facing the frame (Fig. S2) to make it air tight when mounted on the frame. The volume  
161 of the chamber and the part of the frame raised above the surface was 5.3 L. A small fan was  
162 installed inside the chamber to provide good mixing of the air during measurement. A small  
163 weight (stone) was placed on top of the chamber during measurement to prevent it from moving  
164 due to wind gusts. During concentration measurement air was circulated in a closed loop  
165 between the chamber and the gas analyzer in ca. 10 m long 4 mm diameter polyethene tubes (see  
166 Fig. S2). The air flow through the analyzer was ca 1.2 L min<sup>-1</sup>. The chamber was ventilated in  
167 the free air about 1 minute before each measurement which lasted for 5 minutes. The  
168 concentrations were recorded and stored once per second by the gas analyzer. The time stamp of  
169 the recorded data was used to identify measurement cycles for analysis of fluxes.

170

171 The chamber measurement positions were selected in the following way. The frames were  
172 grouped in two sections, one north-east and one south-west of the flux tower since it was  
173 expected that the main wind direction would be along that direction. Each group was then split  
174 into three subsections with four measurement points within each one of them. The locations were  
175 named S1:1-S1:4, S2:1-S2:4, S3:1-S3:4, N1:1-N1:4, N2:1-N2:4 and N3:1-SN3:4. The four  
176 measurement points within each subsection were then placed along a transect with 3-4 m  
177 between each point. This way it was possible to measure all four chamber locations without  
178 having to move the whole measurement system. Chamber measurements were made in three  
179 separate campaigns: mid-summer (26 June to 2 July 2015), late-summer (25-27 August 2015)  
180 and early-summer (14-15 June 2016). Each location was measured three times during each one  
181 of the three campaigns, a total of 216 measurements. Besides gas concentrations, also soil  
182 temperature (5 cm), soil moisture (0-5 cm) and active layer depth was measured during each  
183 campaign.

184

185 Meteorological data needed for analyses and gap-filling were obtained as follows: Hourly air  
186 temperature and relative humidity from Isfjord radio, half-hourly global radiation from  
187 Adventdalen, daily snow depth and ground ice conditions from Svalbard airport and monthly  
188 precipitation from Isfjord radio and Barentsburg. The distance between the measurement site and  
189 these stations are; Isfjord radio, 1 km, Barentsburg, 13 km, Svalbard airport, 46 km and  
190 Adventdalen, 50 km. Data sources are given in Acknowledgement.

191

### 192 **3. Data analysis**

193



194 The rawdata from the eddy covariance flux measurements were analysed using the Eddypro  
195 software version 6.1.0 (Li-Cor, 2016). Correction was made for the impact of the additional heat  
196 flux in the sensor path of the open path analyzer on the flux calculations according Burba et al.  
197 (2008). Gap filling during the measurement period was made using the REddyProc online eddy  
198 covariance data processing tool developed at the Max Planck Institute for Biogeochemistry  
199 (Wutzler et al., 2018) without  $u^*$  correction since we could not identify any threshold for  $u^*$ . The  
200  $u^*$  threshold is generally low for low and smooth vegetation (Pastorello et al., 2020) and for a  
201 wind exposed site as ours, it is not surprising that such threshold could not be found. Only data  
202 of highest quality, i.e. class=0 was retained for the gap filling and further analyses. Gap filling  
203 outside of the EC measurement period to obtain the carbon balance for a full year was made  
204 using empirical relationships for  $R_{eco}$  and GPP (see below).

205  
206 For flux footprint calculations the roughness length ( $z_0$ ) is needed and it was calculated from the  
207 wind profile relationship in near neutral ( $-0.01 < z/L < 0.01$ ) conditions:

$$209 \quad z_0 = \frac{z_m}{e^{(u(z) \cdot \frac{k}{u^*})}} \quad (1)$$

210  
211 where  $z_m$  is measurement height,  $u(z)$  is wind speed at height  $z$ ,  $k$  is von Karman's constant and  
212  $u^*$  is friction velocity. We used the flux footprint prediction (FFP) online tool by Kjun et al.  
213 (2015) to calculate the footprint climatology.

214  
215 The fluxes from the chamber measurements were estimated from the time change of the  
216 concentrations using linear regression. Every individual measurement was inspected and  
217 evaluated manually. These inspections showed that 50 seconds for  $CO_2$  and 100 seconds for  $CH_4$   
218 were optimal to obtain near perfectly linear responses a few seconds after the chamber had been  
219 placed on the frame. The slopes of the regressions were then used to calculate fluxes per unit  
220 surface area. The flux detection limits for  $CO_2$  and  $CH_4$  were calculated in the following way:  
221 first the peak-to-peak variation in the respective gases were determined when the chamber was  
222 ventilated in the free air and when conditions were steady. Then 20 sets of artificial 'fluxes' for  
223 each gas species were estimated based on 100 randomly generated concentrations for each data  
224 set. The peak-to-peak difference was used as seed (input) for the randomly generated values. The  
225 95% value of the distribution of these randomly generated fluxes was taken as the flux detection  
226 limit for the respective gas.

227  
228 The pictures of the vegetation inside of the chamber frames were analysed using the ImageJ  
229 (<https://imagej.net>) public domain software. The camera color channel information (digital  
230 numbers for Red (R), Green (G) and Blue (B) channels) was collected from the JPEG pictures.  
231 This type of pictures is for instance used in studies that are tracking the phenological  
232 development of vegetation (e.g. Richardson et al., 2009). The so-called green index (GI) is  
233 applied to detect differences in greenness of vegetation:

$$235 \quad GI = G / (R + G + B) \quad (2)$$

236



237 This index was also estimated for the central footprint area (100 m radius) of the flux  
238 measurement location using a picture taken at 160 m above the altitude of the measurement area.

239 Forward stepwise linear regression (Sigmaplot 12.5) was used to analyze the dependency of the  
240 CO<sub>2</sub> and CH<sub>4</sub> fluxes on environmental variables. We tested for air temperature (T<sub>a</sub>), soil moisture  
241 (θ), soil temperature (T<sub>s</sub>), active layer depth (ALD), measurement location (S<sub>id</sub>) and GI.

242  
243 For gap filling of R<sub>eco</sub> we only had access to air temperature with full annual coverage and, thus,  
244 we could only use this driver for estimation of the R<sub>eco</sub>. The measured chamber CO<sub>2</sub> fluxes were  
245 fitted to the Lloyd & Taylor (1994) model with air temperature (T<sub>a</sub>) as independent variable:  
246

$$247 \quad FCO_2 = a \cdot e^{b\left(\frac{1}{56.02} - \frac{1}{T_a + 46.02}\right)} \quad (3)$$

248  
249 During the EC measurement period (25 June to 17 September 2015) the GPP was estimated as:  
250

$$251 \quad GPP = NEE_f - R_{eco} \quad (4)$$

252  
253 Where NEE<sub>f</sub> is the gap filled NEE according to Wutzler et al. (2018). This way R<sub>eco</sub> and GPP  
254 become consistent with the measured and gap filled NEE. For the time before and after this  
255 period NEE was estimated as the sum of modelled R<sub>eco</sub> and modelled GPP. The data for the GPP  
256 model was derived from:

$$257 \quad GPP_m = NEE_m - R_{eco} \quad (5)$$

258  
259 Where NEE<sub>m</sub> is the measured net ecosystem exchange. The GPP<sub>m</sub> was then fitted to a light  
260 response function:

$$261 \quad GPP_m = c1 + c2 \cdot c3 / (c2 + R_g) \quad (6)$$

262  
263  
264

## 265 **4 Results**

266 For CO<sub>2</sub> exchanges and partitioning we combined the soil efflux measurements with the chamber  
267 system with the eddy covariance flux measurements. This was crucial for the partitioning and for  
268 gap filling because from 20 April to 20 August at this location the sun is above the horizon 24  
269 hours of the day and this means that there were few occasions of dark nighttime measurements  
270 with the eddy covariance system and all of these were collected at the very end of the summer.  
271 We consider the chamber measurements that were distributed across the summer to be more  
272 representative of R<sub>eco</sub> for this location.

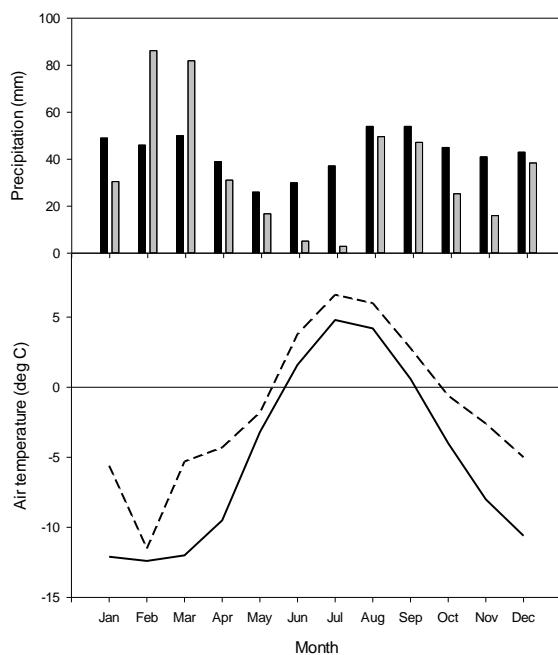
273  
274 For CH<sub>4</sub> exchanges we don't have any eddy covariance measurements so we present only  
275 chamber data for this variable.

### 276 **4.1 Weather**

277  
278  
279 The mean annual temperature at Kapp Linne was -1.5 °C during 2015 which was 3.5 °C higher  
280 than the long-term mean (1961-1990) of -5.1 °C. The summer (June-August) mean of 5.5 °C was



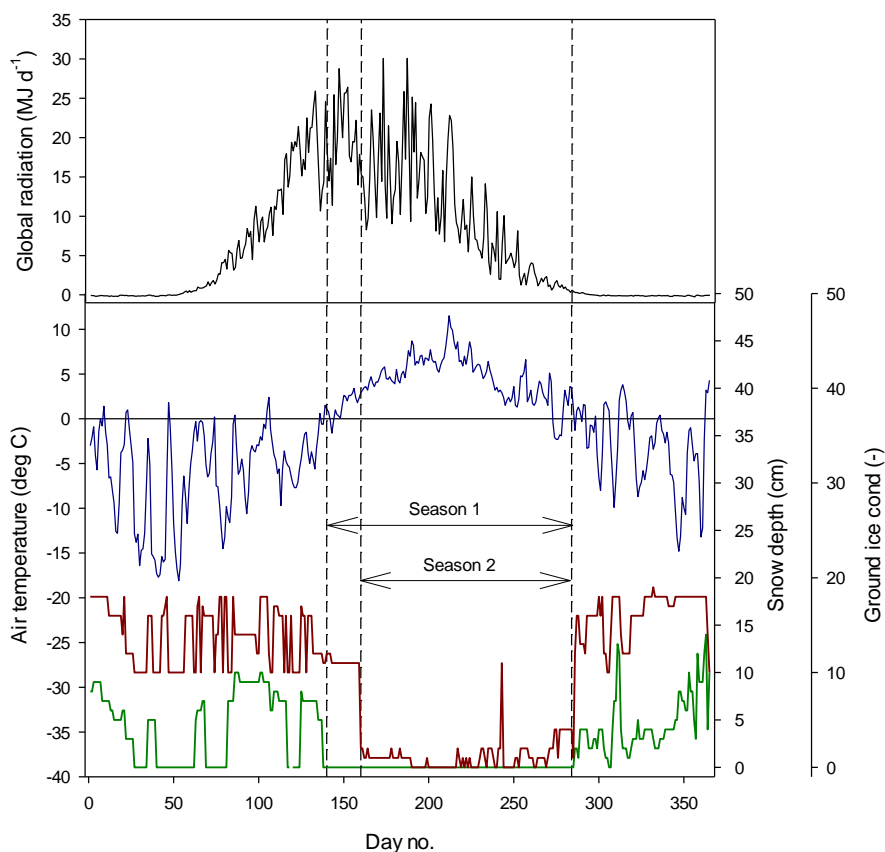
281 2.0 °C higher than the long-term mean for the same time period (Fig. 1). The summer  
282 precipitation in 2015 was much lower, 58 mm as compared to the long-term precipitation which  
283 was 121 mm. The annual precipitation was also lower, 431 mm compared to the long-term  
284 precipitation which was 514 mm.



285 Figure 1. Monthly precipitation (top): Long-term average 1961-1990 black bars and 2015 grey  
286 bars. Data from Barentsburg for January-May, from Isfjord Radio for June-December. Mean  
287 monthly air temperature (bottom): Solid line is long-term average 1961-1990 and dotted line is  
288 2015. Data from Isfjord Radio which is located about 1 km west of the investigation area.  
289

290  
291 We defined the start of the growing season (the period during which vegetation is  
292 photosynthesizing) in two different ways. The first (denoted Season 1, day no. 140; see Fig. 2)  
293 based on when daily air temperature started to stay above zero more steadily and the second  
294 (denoted Season 2, day no. 160) when most of the snow had disappeared. The ending of the  
295 growing season was defined as when the air temperature fell more steadily below zero, when  
296 ground ice began to establish and when a significant snow pack was established (day no. 284;  
297 Fig. 2).

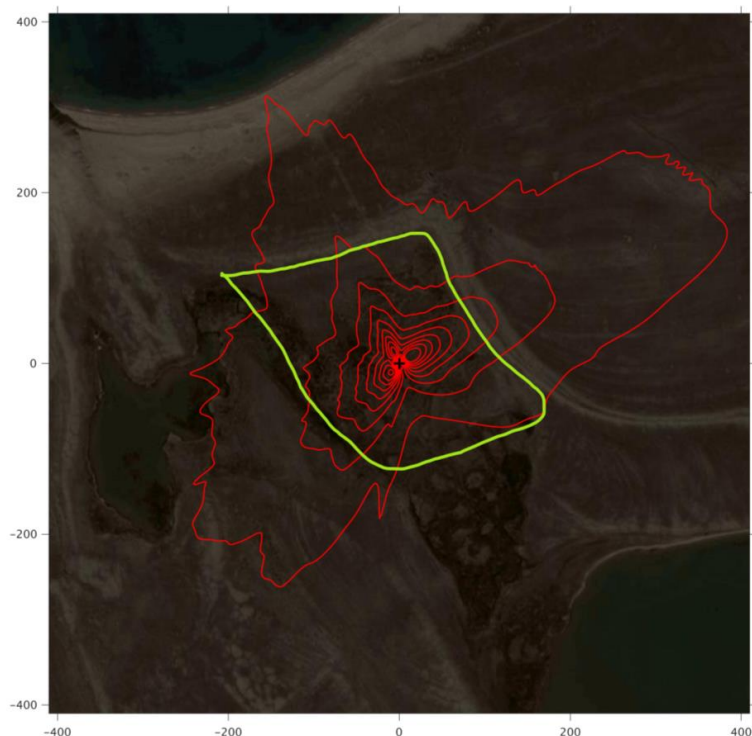




298  
299 Fig. 2 Weather conditions during 2015. Top panel: Mean daily global radiation at Adventdalen.  
300 Bottom panel: Mean daily air temperature at Isfjord Radio (blue), snow depth (red) and ground  
301 ground ice conditions (green) at Svalbard airport close to Longyearbyen. The ground ice condition is  
302 scaled from 0 to 20 where 0 is no snow or ice on the ground and 20 indicate a complete cover of  
303 snow or ice.

#### 304 305 4.2 Flux footprint and greenness

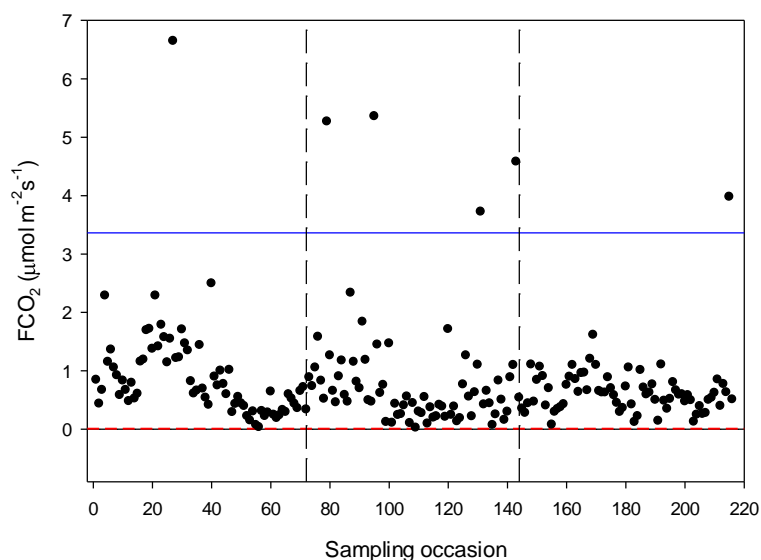
306  
307 The footprint climatology shows a good representativity of the moss tundra surface by the EC  
308 measurements with 60-70% of fluxes emanating from areas well within the border of the tundra  
309 (Fig. 3). The mean green index for a circular area with radius of 100 m centered at the flux tower  
310 was 0.34 which corresponded exactly to the mean value for all chamber locations. The GI for the  
311 24 chamber locations varied between 0.316 and 0.369. We observed a good (visual) correlation  
312 between GI and coverage of green plants (see Figures S4a-S4y of chamber location pictures and  
313 GI).  
314



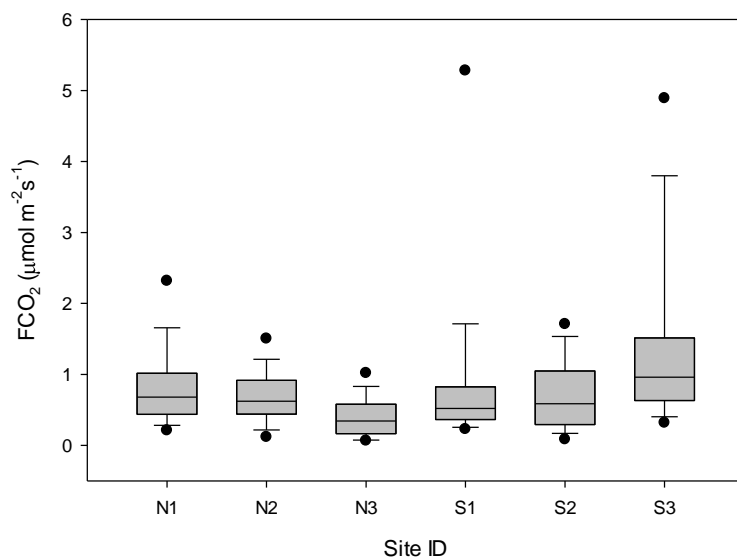
315  
316 Figure 3. The footprint climatology with red contour lines 10-90%. The area within the green  
317 line mark the heart of the moss tundra. The scale (m) is shown on the outer borders of the  
318 picture.

319  
320 4.3 CO<sub>2</sub> exchanges

321  
322 The CO<sub>2</sub> fluxes from the chamber measurements showed quite large variation over time (Fig. 4)  
323 and across sampling locations (Fig. 5). The mean CO<sub>2</sub> flux of all samples was  $0.81 \pm 0.11 \mu\text{mol}$   
324  $\text{m}^{-2}\text{s}^{-1}$ . The uncertainty is given as the 95 confidence limit.  
325



326  
327 Figure 4. Measured CO<sub>2</sub> exchange from the 24 sampling points using dark chamber and portable  
328 gas analyzer. The dashed red line indicates CO<sub>2</sub> flux detection limit and the blue line represents  
329 3xS.D. of all data points. The dashed vertical lines separate sampling periods from left to right:  
330 early summer, mid-summer and late-summer.



331  
332 Figure 5. Box plot of CO<sub>2</sub> fluxes per sampling location named N1-N3, S1-S3. The boundaries of  
333 the grey boxes represent the 25% and 75% percentiles, the line represent the median, whiskers  
334 above and below the boxes indicate the 10% and 90% percentiles. Outlying points are also  
335 shown.



336

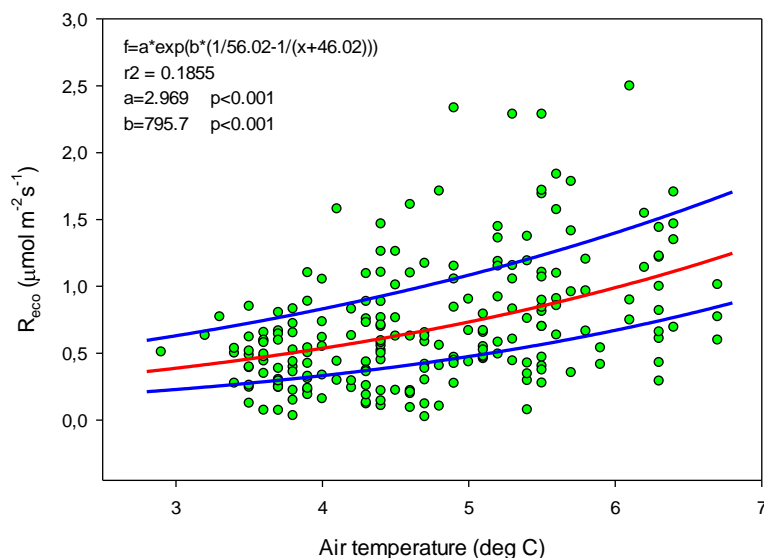
337 Of the tested environmental variables  $T_a$ ,  $\theta$ ,  $T_s$ , ALD,  $S_{id}$  and GI it was only  $T_a$ ,  $\theta$  and GI that  
 338 contributed positively and significantly in decreasing order to explain the variability of the  $CO_2$   
 339 flux (Table 1).  
 340

341 Table 1. Result of stepwise linear regression with  $CO_2$  flux as dependent variable. Normality test  
 342 failed but significance in all variables was confirmed with Wilcoxon Signed rank tests.  
 343

Variable	Partial- $R^2$	Probability (p)
$T_a$	0.190	<0.001
$\theta$	0.037	0.002
GI	0.023	0.002

344

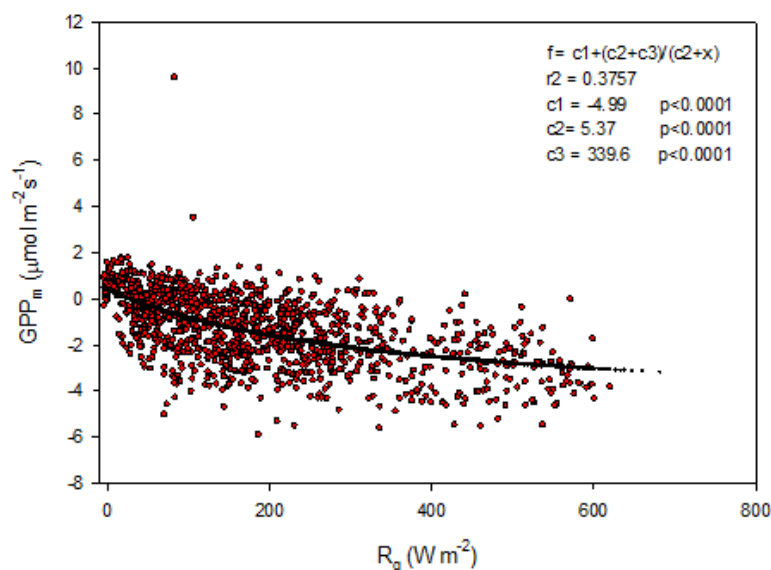
345 Ideally all of these variables should be used in a model to estimate  $R_{eco}$  for gap filling purposes  
 346 but we could only use air temperature since this was the only variable that we had access to with  
 347 complete coverage for a full year. The Lloyd & Taylor model (Eq. 3 & Fig. 6)) was thus used to  
 348 estimate ecosystem respiration for 2015 using half-hourly air temperature as input.



349

350 Figure 6. Measured ecosystem respiration (green dots) plotted against air temperature. The red  
 351 curve is the fitted equation and the blue curves are the corresponding boundaries when  
 352 considering the standard deviation of the parameters.  
 353

354 The modelled gross primary productivity (Eq. 6;  $GPP_m$ ) had a small offset when global radiation  
 355 was zero (Fig. 7). This offset was adjusted for when the model was applied for gapfilling so that  
 356 GPP become zero during nighttime.



357  
358

359 Figure 7.  $GPP_m$  plotted against global radiation; red symbols are estimated values according to  
360 eq. (5) and the black symbols are the fitted model.

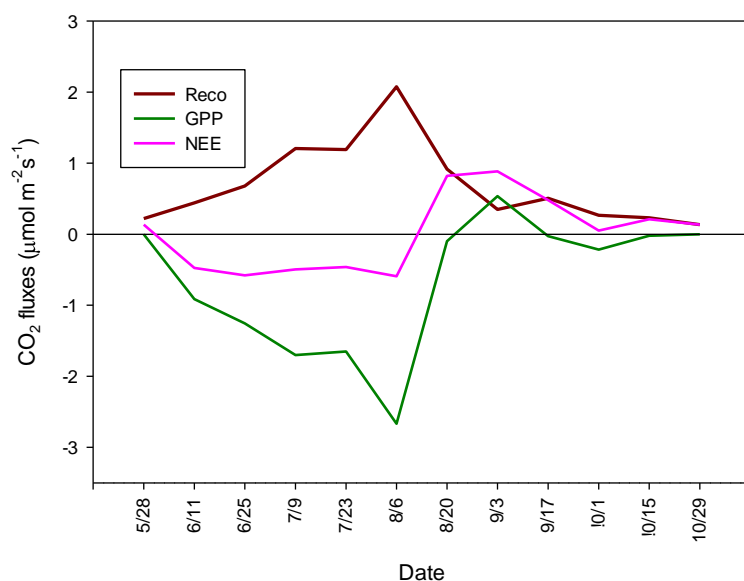
361

362 We assumed that GPP was zero for the periods outside of the growing season and that our  $R_{eco}$   
363 model was valid during winter as well as during growing season. However, during winter the air  
364 temperature is not the appropriate driver for respiration because of the insulating effect of the  
365 snow cover. We did not have access to soil temperature from our site but data from Adventdalen  
366 which is located about 60 km east from our site, showed that the soil surface temperature was  
367 close to zero degrees below the snow pack during the winter (N. Pirk, unpublished data). Thus,  
368 we assumed that the situation would be similar in our site and used zero degrees as driver for  
369 respiration.

370

371 The mean bi-weekly fluxes show that NEE is negative from about one week into June until one  
372 week into August (Fig. 8). The mean NEE is relatively constant during this period with a low -  
373  $0.5 \mu\text{mol m}^{-2}\text{s}^{-1}$ . The maximum bi-weekly GPP is about  $-2.5 \mu\text{mol m}^{-2}\text{s}^{-1}$  while the corresponding  
374  $R_{eco}$  is about  $2.0 \mu\text{mol m}^{-2}\text{s}^{-1}$ . The GPP become positive during one period in the autumn  
375 indicating an underestimation of  $R_{eco}$  during that time.

376



377  
 378 Figure 8. Bi-weekly gap filled CO<sub>2</sub> fluxes for season 2 (see Fig. 2) at Tunsjömyren, Kapp Linne  
 379 during 2015.

380  
 381 The annual modelled and gap filled NEE was negative, -12.4 g C m<sup>-2</sup> for season 1 and positive,  
 382 24.7 g C m<sup>-2</sup> for season 2. The gapfilled NEE (Table 2) during the summer (June-August) was -  
 383 37 g C m<sup>-2</sup> or -0.40 g C m<sup>-2</sup> day<sup>-1</sup> which is good agreement with the measured NEE (25 June -31  
 384 August) with a mean daily uptake of -0.40 g C m<sup>-2</sup> day<sup>-1</sup>. A summary of all components for the  
 385 different seasons are presented in Table 2.

386  
 387 Table 2. Summary of annual and seasonal C-fluxes from Kapp Linne.

388

Period	Component (g C m <sup>-2</sup> )	Season	
		1	2
Winter	Reco	29.5	31.5
	GPP	0	0
	NEE	29.5	31.5
Growing season	Reco	114.9	109.5
	GPP	-156.8	-116.3
	NEE	-41.9	-6.8
Summer (June-August)	Reco	97.8	97.8
	GPP	-134.8	-134.8
	NEE	-37.0	-37.0
Annual	Reco	144.4	141.0
	GPP	-156.8	-116.3
	NEE	-12.4	24.7



389

390

#### 4.4 Temperature sensitivity of $R_{eco}$ and GPP

391

392

393

394

395

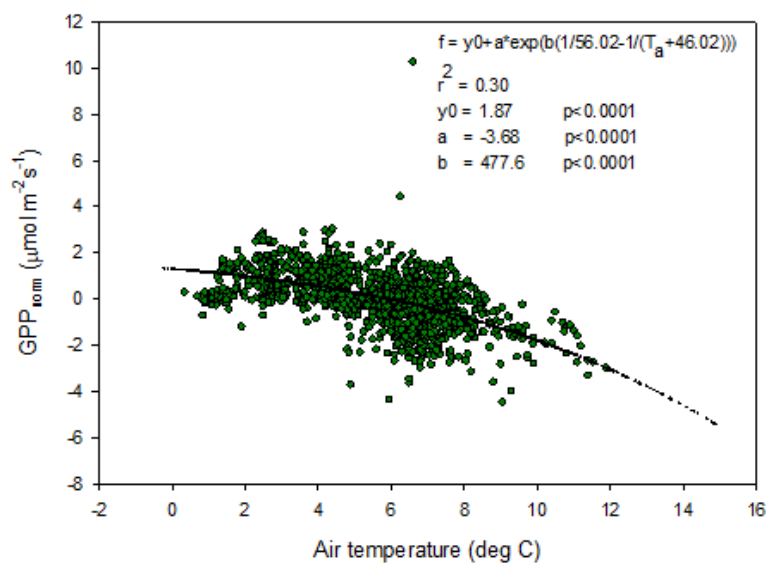
396

397

398

399

The temperature sensitivity of the  $R_{eco}$  is already given by the fitted Lloyd & Taylor (1994) equation. In the absence of long time series of measurements during multiple year were natural climate variability could be used to assess temperature sensitivity of GPP we approached this problem in the following way. We normalize GPP for its dependence on radiation by estimating the difference between the ‘measured’ GPP and the model which only depends on radiation (see Fig. 7). The resulting normalized GPP show a dependence on air temperature (Fig. 9) with values becoming more negative with increasing temperature. We fitted the same type of model to these data as for the  $R_{eco}$  to be able to compare sensitivities to temperature.

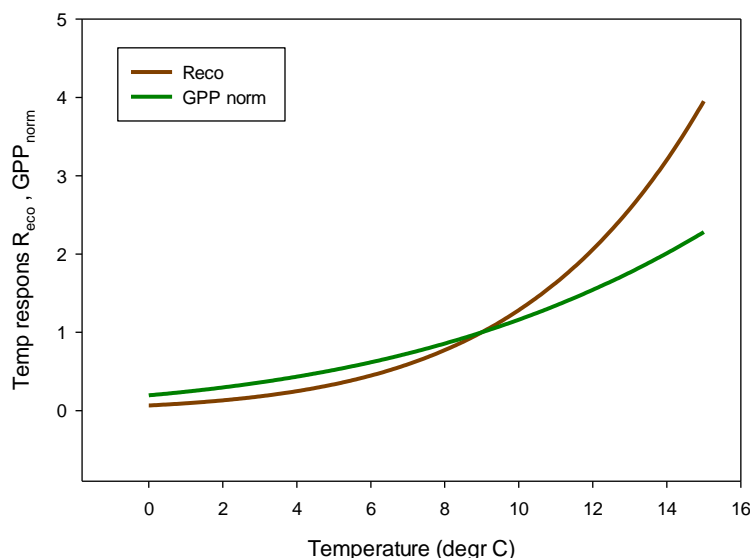


400

401

402

Figure 9. Normalized GPP plotted against air temperature and with the fitted exponential model.



403 Figure 10. Temperature sensitivity for  $R_{\text{eco}}$  (brown) and  $R_{\text{g}}$ -normalized (positive) GPP (green).  
404  
405

406 In Fig. 10 we reversed the sign of the GPP temperature response function to make it more easily  
407 comparable with the  $R_{\text{eco}}$  response model. The temperature sensitivity ( $\mu\text{mol m}^{-2}\text{s}^{-1} \text{K}^{-1}$ ) can be  
408 estimated from the slope of these curves and the sensitivity is slightly higher for GPP than for  
409  $R_{\text{eco}}$  in the interval 0 – 4.5 °C, thereafter the difference is small up to about 7 °C then it began to  
410 raise rapidly for  $R_{\text{eco}}$ . We tested what impact this could have by increasing the measured half-  
411 hourly air temperature by 1 °C and found that during the growing season (season 2) the GPP  
412 increased by  $-3.89 \text{ g C m}^{-2}$  and  $R_{\text{eco}}$  by  $3.53 \text{ g C m}^{-2}$ . Thus, a minor increase of GPP compared to  
413  $R_{\text{eco}}$ . However, a one-degree higher winter temperature resulted in an addition respiration of  $9 \text{ g C m}^{-2}$ .  
414 Thus, an estimated loss of  $8.5 \text{ g C m}^{-2}$  for the whole year.  
415

#### 416 4.5 CH<sub>4</sub> exchanges

417

418 The CH<sub>4</sub> fluxes from the chamber measurements showed large variation over time (Fig. 11) and  
419 across sampling locations (Fig. 12). The mean CH<sub>4</sub> flux of all samples was  $0.00051 \pm 0.00024$   
420  $\mu\text{mol m}^{-2}\text{s}^{-1}$ . The uncertainty is given as the 95% confidence limit. Setting all fluxes that fell  
421 within the flux detection limits to zero changed the mean value with  $-0.2\%$ . Assuming that the  
422 mean flux was representative for the whole of growing season 1, the total CH<sub>4</sub> summer emission  
423 was  $0.039$  to  $0.164 \text{ g CH}_4 \text{ m}^{-2}$ . Converting this to CO<sub>2</sub>-equivalents (CO<sub>2</sub>-eq) we get a range of 1.1  
424 to  $4.6 \text{ g CO}_2\text{-eq}$  for the summer and if we add also a possible winter emission of 22% of the  
425 annual (following Bao et al., 2021) we obtain an annual mean of  $3.2 \pm 2.0 \text{ g CO}_2\text{-eq}$  using a  
426 GWP<sub>100</sub> of 27.9 (Arias et al., 2021). The corresponding value using GWP<sub>20</sub> of 81.2 (Arias et al.,  
427 2021) is  $9.3 \pm 5.8 \text{ g CO}_2\text{-eq}$  for the annual emission.  
428

429 We also noticed a clear trend during the summer with highest fluxes in mid-June and then  
430 decreasing during the following two sampling occasions. The respective mean values with 95%





431 confidence intervals for the three sampling periods were  $0.00121 \pm 0.000512 \mu\text{mol m}^{-2}\text{s}^{-1}$  (June 14-  
432 15),  $0.000332 \pm 0.000465 \mu\text{mol m}^{-2}\text{s}^{-1}$  (June 26- July 2) and  $-0.00000781 \pm 0.0000936 \mu\text{mol m}^{-2}\text{s}^{-1}$   
433 (August 25-26).

434

435 For  $\text{CH}_4$  exchanges we found *ALD*,  $\theta$  and *GI* to contribute significantly to explain the variance of  
436 the flux (Table 3). The  $\text{CH}_4$  flux responded negatively to increasing *ALD* and positively to  $\theta$  and  
437 *GI*.

438

439 Table 3. Result of stepwise multiple linear regression with  $\text{CH}_4$  flux as dependent variable.

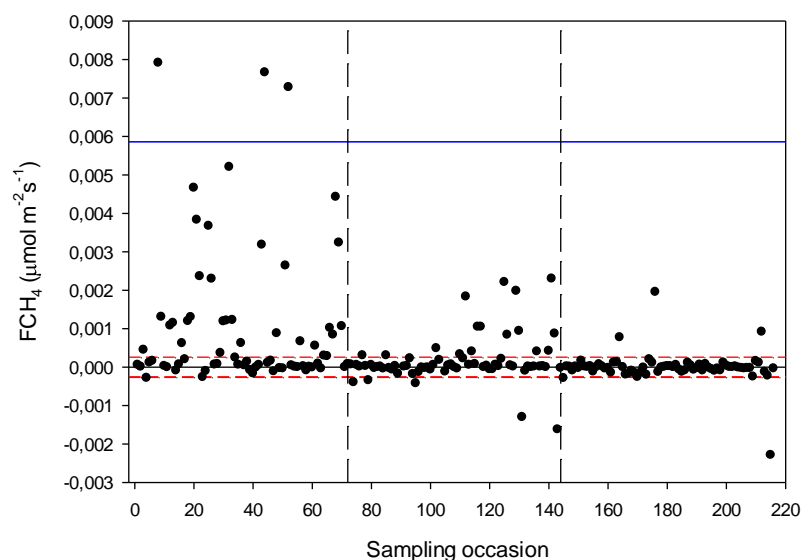
440 Normality test failed but significance in all variables was confirmed with Wilcoxon Signed rank  
441 tests.

442

Variable	Delta-R <sup>2</sup>	Probability (p)
ALD	0.175	<0.001
$\theta$	0.025	0.01
GI	0.020	0.004

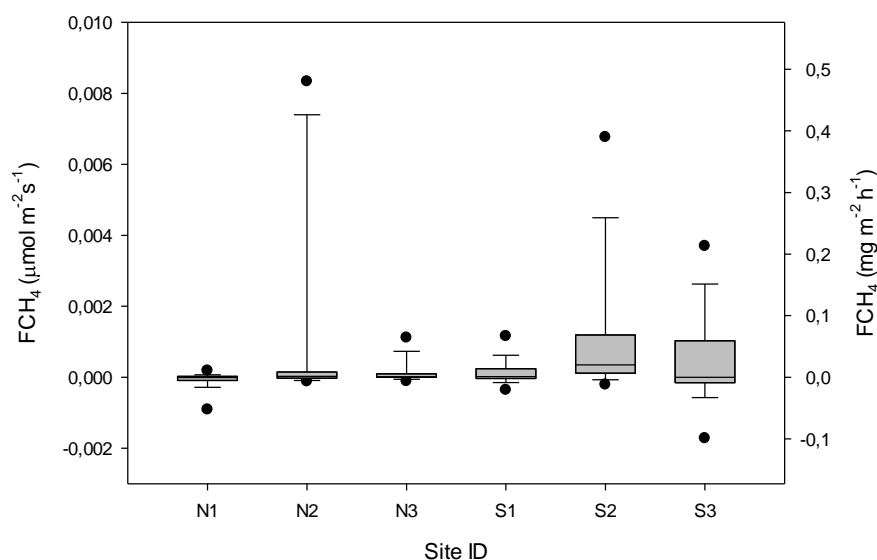
443

444



445

446 Figure 11. Measured  $\text{CH}_4$  exchange from the 24 sampling points using dark chamber and  
447 portable gas analyzer. The dashed red lines indicate  $\text{CH}_4$  flux detection limit, (i.e. inside the  
448 limits of detection the exact numbers are highly uncertain) and the blue line represents  $3 \times \text{S.D.}$   
449 The dashed vertical lines – same as in Fig. 4.



450

451 Figure 12. Box plot of CH<sub>4</sub> fluxes per sampling location named N1-N3, S1-S3. The statistics  
452 includes also the data that fall within the flux detection limits. The boundaries of the grey boxes  
453 represent the 25% and 75% percentiles, the line represent the median, whiskers above and below  
454 the boxes indicate the 10% and 90% percentiles. Outlying points are also shown.

## 455 5 Discussion

### 456 5.1 Annual and seasonal CO<sub>2</sub> fluxes

457

458 We focus our discussion mainly on comparison with other tundra sites located in the North  
459 Atlantic area since these sites are influenced by the North Atlantic Current with its impact on  
460 weather patterns and climate. This limits the comparisons to sites in Greenland, Svalbard and  
461 Northern Scandinavia. However, we broaden the comparison a bit by adding two sites from  
462 Alaska.

463

464 Our annual NEE was in the range -12.4 to 24.7 g C m<sup>-2</sup> depending on definition of growing  
465 season (Table 2). We judge the latter value to be more realistic since season 1 includes an  
466 unrealistically high GPP when there is still a snow cover on the ground in early spring. We used  
467 the high and low estimates of the fitted functions for R<sub>eco</sub> (see Fig. 6) to assess the sensitivity of  
468 annual NEE to uncertainty in winter respiration and we found the range to be between 17.1 g C  
469 m<sup>-2</sup> to 32.9 g C m<sup>-2</sup>.

470

471 Lund et al. (2012) found that the start of the uptake period was strongly correlated with start of  
472 the snowmelt for the fen in Zackenberg, NE Greenland. They defined the start of snowmelt as  
473 the day when snow depth was <0.1 m. This coincides very well with our definition of start of  
474 growing season 2 (see Fig. 2). Soegaard and Nordtroem (1999) reported an annual NEE of -64.4  
475 g C m<sup>-2</sup> for the fen in Zackenberg and Pirk et al. (2017) reported -82 g C m<sup>-2</sup> for an alluvial fen in



476 Adventdalen, Svalbard, not far from Kapp Linne. For a site on the west coast of Greenland,  
477 Disco island with heath vegetation, Zhang et al. (2019) reported an annual NEE of  $-25 \pm 15$  g C  
478  $\text{m}^{-2}$ . Christensen et al. (2012) reported a range of  $-20$  to  $-95$  g C  $\text{m}^{-2}$  for annual NEE in a palsa  
479 mire in Abisko, Northern Sweden. Our results are closer to the values found for a sparsely  
480 vegetated catchment area in Bayelva, Ny-Ålesund where Lüers et al. (2014) reported annual NEE  
481 to be 0 g C  $\text{m}^{-2}$ . If we go beyond the North Atlantic area to the low Arctic region in North  
482 America we can find sites that has a positive NEE on annual basis, 13.6 g C  $\text{m}^{-2}$  for a tussock  
483 tundra near Atquasuk, Alaska (Oechel et al., 2013) and 21-61 g C  $\text{m}^{-2}$  for a heath and 2-82 g C  
484  $\text{m}^{-2}$  for a wet sedge ecosystem in Innvait creek (Eurkirchen et al., 2012).

485  
486 Lund et al. (2012) analysed 10 years of EC flux measurements from a heathland in Zackenberg  
487 and they reported a NEE range of  $-39.7$  to  $-4.3$  g C  $\text{m}^{-2}$  for the growing season. Our result for the  
488 growing season NEE of  $-6.8$  g C  $\text{m}^{-2}$  (Season 2; Table 2) fall within the same range but it was  
489 only two years out of ten that showed that low uptake in Zackenberg heath. Their measured  
490 growing season GPP was in the range of  $-95.4$  to  $-54.1$  g C  $\text{m}^{-2}$  and the  $R_{\text{eco}}$  was in the range of  
491  $37.7$  to  $63.8$  g C  $\text{m}^{-2}$ . Our corresponding values were  $-116.3$  g C  $\text{m}^{-2}$  for GPP and  $109.5$  g C  $\text{m}^{-2}$   
492 for  $R_{\text{eco}}$ . López-Blanco et al. (2017) presented data over a period of eight years of EC flux  
493 measurements from Kobbefjord, SW Greenland over an area of mixed fen and heath vegetation.  
494 Their growing season ranges were; for NEE  $-74.2$  to  $-45.9$  g C  $\text{m}^{-2}$ , for GPP  $-316.2$  to  $-181.8$  g  
495 C  $\text{m}^{-2}$  and for  $R_{\text{eco}}$  it was  $144.2$  to  $279.2$  g C  $\text{m}^{-2}$  excluding 2011 which was anomalous because  
496 of a pest outbreak and 2014 which did not have a full growing season.

497  
498 Our EC measurements of summer (June-August) NEE of  $-37$  g C  $\text{m}^{-2}$  (Table 2) is in-between  
499 ranges reported for fen type of vegetation in NE Greenland;  $-96.3$  g C  $\text{m}^{-2}$  (Soegaard and  
500 Nordstroem 1999) to  $-50$  g C  $\text{m}^{-2}$  (Rennermalm et al. 2005) and heath vegetation;  $-1.4$  to  $-18.9$  g  
501 C  $\text{m}^{-2}$  (Groendahl et al. 2007).

502  
503 It is difficult to compare growing season values because they are rarely defined the same way.  
504 Only small differences in definition of start and end of growing season can have a large impact  
505 on the NEE values since NEE is the sum of two large components of almost equal size and of  
506 different sign. In our case a 20 days difference in the beginning of the season changes growing  
507 season NEE from  $-12.4$  to  $24.7$  g C  $\text{m}^{-2}$ . It is also difficult to compare GPP and  $R_{\text{eco}}$  for any  
508 season since the methods to split NEE into components differ from case to case. The most  
509 reliable comparison is probably for summer season (June – August) since most studies represents  
510 this period best in terms of measurement coverage and quality. So, with this in mind we are  
511 pretty confident with placing the C-exchange rates of the moss tundra intermediate between fen  
512 and heath type of vegetation in the North Atlantic region.

## 513 514 5.2 CH<sub>4</sub> fluxes 515

516 Our estimated growing season CH<sub>4</sub> flux of  $0.08$  g C  $\text{m}^{-2}$  is very low compared to most other  
517 methane emitting tundra sites; the Zackenberg fen site emitted CH<sub>4</sub> in the range  $1.4$  to  $4.9$  g C  $\text{m}^{-2}$   
518 (Mastepanov et al. (2013), Jackowicz-Korczynski et al. (2010) reported  $20.1$  to  $25.1$  g CH<sub>4</sub>  $\text{m}^{-2}$   
519 for the Stordalen mire in Northern Sweden. For three different sites in northern Alaska, Bao et  
520 al. (2021) reported annual emissions between  $1.8$  and  $8.5$  g CH<sub>4</sub>  $\text{m}^{-2}$  which corresponds to  $0.94$   
521 and  $4.5$  g CH<sub>4</sub>  $\text{m}^{-2}$  for the growing season based on their estimate that growing season emissions



522 are 52.6% of the annual emissions. Sachs et al. (2008) measured CH<sub>4</sub> exchanges with EC method  
523 in a northern Siberian polygon tundra and found generally low fluxes of about 18.5 mg CH<sub>4</sub> m<sup>-2</sup>  
524 day<sup>-1</sup> with little variation over the growing season. This rate adds up to 2.3 g CH<sub>4</sub> m<sup>-2</sup> for their  
525 four months long growing season.

526  
527 It should be pointed out that we did not perform measurements during the shoulder seasons  
528 meaning that we probably underestimate the seasonal total. Importance of shoulder seasons was  
529 first pointed out by Mastepanov et al. (2008) which discovered a large burst of CH<sub>4</sub> at and after  
530 the onset of soil freezing. One interesting observation is that the main part of our CH<sub>4</sub> flux  
531 occurred during the sampling period 14-15 June 2016 which is about 30 days after snow melt.  
532 This is the time of the season when CH<sub>4</sub> emissions normally are peaking (Mastepanov et al.  
533 2013). After that, the rates dropped to practically zero in late August (see Fig. 11).

534  
535 If we sum up the annual net CO<sub>2</sub> and CH<sub>4</sub> fluxes expressed as CO<sub>2</sub>-eq we find that the moss  
536 tundra is emitting in total 60 g CO<sub>2</sub>-eq of which the methane stands for 7%. So even if the CH<sub>4</sub>  
537 fluxes are small, it still represents a significant global warming impact in relative terms.

538  
539 The comparison between the different sites are hampered by the fact that they in most cases  
540 belong to different bioclimatic subzones with differences in climate and vegetation (Walker et  
541 al., 2005). The only site besides Kapp Linne that belong to subzone B is the one in Ny Ålesund.  
542 The other high Arctic sites Adventdalen and Zackenberg both belong to subzone C, the  
543 intermediate high/low Arctic sites Kobbefjord and Disco Island belongs to subzone D  
544 respectively C/D. The low Arctic site Atqasuk belong to subzone D and the Imnavait Creek  
545 belong to subzone E. The sub-Arctic Abisko is not classified by Walker et al. (2005) but based  
546 mean July air temperature it should belong to subzone E. These differences in climate and  
547 vegetation should be kept in mind when comparing results from different sites.

### 548 549 5.3 Environmental controls of fluxes

550  
551 A key issue in high Arctic is how ecosystems with soil that contain large amounts of frozen  
552 carbon will respond to warming. A recent report about the future climate of Svalbard (Hanssen-  
553 Bauer et al. 2019) show that appalling changes are at risk to occur. By 2071-2100 compared to  
554 1971-2000 the mean annual temperature is estimated to increase by 7 °C to 10 °C for the medium  
555 and high emission scenarios, respectively. Precipitation is also estimated to increase by 45%  
556 respectively 65% for these scenarios. Such large changes will of course also have a lot of other  
557 impacts as well for instance shorter snow season, more erosion and sediment transport, changes  
558 in vegetation composition and growth etc etc. Assessment of such large changes are very  
559 difficult and is far beyond the scope of this paper. We have however shown that for a smaller  
560 temperature increase of 1 degree, the impact on the net carbon balance during the growing  
561 season will be minute; the increase in ecosystem respiration is compensated for by a  
562 corresponding, or actually slightly larger increase of gross primary productivity. Similar  
563 compensation effect was obtained for a heath site in Zackenberg by Lund et al. (2012). They  
564 used multi-year measurements to assess the effect of changes in temperature on the growing  
565 season fluxes. But, if we also consider an increase in temperature during winter, it is most likely  
566 that the annual NEE becomes weakened. It is not unlikely that the impact of climate change with



567 higher temperature that is already a reality in Svalbard can be the reason why the annual NEE  
568 now is positive, i.e. the moss tundra is a GHG source of CO<sub>2</sub> to the atmosphere.

569  
570 We found that air temperature was the main control of ecosystem respiration followed by soil  
571 moisture and greenness index (Table 1). We had expected that soil temperature should contribute  
572 significantly to explain the variations in R<sub>eco</sub> but it did not. Cannone et al. (2019) showed that  
573 ground surface temperature at 2 cm depth contributed significantly to explain R<sub>eco</sub> in nearby  
574 Adventdalen during early, peak and late parts of the growing season. In their study soil moisture  
575 was also significant during peak and late seasons. One possible explanation to this difference in  
576 responses could be that our soil temperature was measured at 5 cm depth and that air temperature  
577 was more representative for the microbial processes taking place in or near the soil surface.  
578 Interestingly, GI contributed significantly to explain variations in R<sub>eco</sub>. The GI was clearly  
579 correlated with the abundance of *Salix polaris* (see Supplement) and thus we interpret the  
580 positive correlation between GI and R<sub>eco</sub> to be an effect of increasing contribution by autotrophic  
581 respiration to the total respiration.

582 We found no significant correlation between CH<sub>4</sub> emission and temperature. The best  
583 explanation was by active layer depth followed by soil moisture and GI (Table 3). But it should  
584 be pointed out that ALD and  $\theta$  are not independent from each other and that ALD can be  
585 regarded as a proxy for any seasonal variability, like plant phenology. Soil moisture decreases  
586 with increasing active layer depth. The correlation between GI and CH<sub>4</sub> emission is probably  
587 also connected with abundance of *Salix polaris* which is a vascular plant. Vascular plants are  
588 since long mentioned as a pathway for CH<sub>4</sub> from the soil interior to the atmosphere in wet tundra  
589 ecosystems (e.g. Schimel, 1995) but it could also be an effect of mediation of soil by the root  
590 exudation of organic acids as mentioned by Ström et al. (2012). However, we have not found any  
591 studies supporting the latter hypothesis concerning *Salix polaris*.

## 592 **6 Conclusions**

593 Our analyses of EC and chamber flux measurements have shown that the moss tundra on Kapp  
594 Linne is a small source of CO<sub>2</sub> and an even smaller source of CH<sub>4</sub> on an annual basis.  
595 Concerning the magnitude of the CO<sub>2</sub> exchanges during summer we find it to be in between  
596 those of fens and heath ecosystems located in the North Atlantic region. The CH<sub>4</sub> exchange is  
597 much lower than for other tundra ecosystems in the region.

598  
599 The temperature sensitivity for CO<sub>2</sub> exchange was slightly higher for GPP than for R<sub>eco</sub> in the  
600 low temperature range of 0-4.5 °C, almost similar up to 7 °C and thereafter it was considerably  
601 higher for R<sub>eco</sub>. The consequence of this, for a small increase in air temperature of 1 degree (all  
602 other variables assumed unchanged) was that the increases in the two fluxes practically evened  
603 out during the growing season. But a warmer winter period would probably result in an increased  
604 loss of carbon. We cannot rule out that the reason why the moss tundra is a net source today is an  
605 effect of the warming that has already taken place in Svalbard.

606 The analysis of which environmental factors that controlled the small-scale fluxes showed that  
607 air temperature dominated for R<sub>eco</sub> and active layer depth for CH<sub>4</sub> but we also found that  
608 greenness index significantly explained part of the variation in these fluxes. For R<sub>eco</sub> we  
609 attributed this to an increased share of autotrophic respiration to the total and for CH<sub>4</sub> we



610 hypothesized that the abundance of the woody shrub *Salix polaris* effected the exchange either  
611 through internal plant pathway for methane or through increased provision of C substrate to the  
612 anaerobic microbial community stimulating the production of methane. This finding is an  
613 indication that modeling of CO<sub>2</sub> as well as of CH<sub>4</sub> fluxes can be improved by also considering  
614 differences and changes in greenness of the vegetation.

## 615 **7 Supplement**

616 The supplement contains some additional photographs of equipment, site and color photographs  
617 of vegetation within the frames used for chamber measurements.

## 618 **8 Data availability**

619 Data can be obtained from <https://zenodo.org> ([10.5281/zenodo.5704508](https://zenodo.org/record/5704508)).

## 620 **9 Author contribution**

621 AL designed the study and wrote the manuscript. NP and AL performed the EC measurements  
622 and analysed the EC data. ISJ did the vegetation characterization. AL, CS, LK and MBN  
623 performed the chamber measurements. All authors have read and commented the manuscript.

## 624 **10 Competing interests**

625 We declare no competing interests.

## 626 **11 Acknowledgments**

627 This work did not receive any other funding except salaries for the authors from their respective  
628 organizations. Observations of air temperature, relative humidity, precipitation, ground ice  
629 conditions and snow depth were obtained from Norwegian Centre for Climate Services (NCCS)  
630 and provided under licence CC BY 4.0. Global radiation data from Adventdalen was obtained  
631 from the University Centre in Svalbard (UNIS). Thanks to associated professor Jonas Åkerman,  
632 Lund University for support with information about the site.  
633

## 634 **12 References**

- 635 Arias, P. A., Bellouin, E., Coppola, R.G. et al.: Technical Summary, in: Climate Change 2021:  
636 The Physical Science Basis. Contribution of Working Group I to the Sixth Assessment  
637 Report of the Intergovernmental Panel on Climate Change, edited by: Masson-Delmotte,  
638 V., P. Zhai, A. Pirani, S. L. Connors, C. Péan, S. Berger, N. Caud, Y. Chen, L. Goldfarb,  
639 M. I. Gomis, M. Huang, K. Leitzell, E. Lonnoy, J.B.R. Matthews, T. K. Maycock, T.  
640 Waterfield, O. Yelekçi, R. Yu and B. Zhou, Cambridge University Press, In Press, 2021.
- 641 Bao, T., Xu, X., Jia, G., Billesbach, D.P. and Sullivan, R.C.: Much stronger tundra methane  
642 emissions during autumn freeze than spring thaw, *Global Change Biology*, 27, 376–387,  
643 [https://doi.org/ 10.1111/gcb.15421](https://doi.org/10.1111/gcb.15421), 2021
- 644 Bosiö, J., Stiegler, C., Johansson, M., Mbufong, H. N. and Christensen, T. R.: Increased  
645 photosynthesis compensates for shorter growing season in subarctic tundra—8 years of



- 646 snow accumulation manipulations, *Climatic Change*, 127, 321–334,  
647 <http://doi.org/10.1007/s10584-014-1247-4>, 2014.
- 648 Burba, G. G., McDermitt, D., Grelle, A., Anderson, D.J. and Xu, L.: Addressing the influence of  
649 instrument surface heat exchange on the measurements of CO<sub>2</sub> flux from open-path gas  
650 analyzers, *Global Change Biology*, 14, 1854–1876, <https://doi.org/10.1111/j.1365-2486.2008.01606.x>, 2008.
- 652 Callaghan, T.V., Björn, L.O., Chapin III, F.S., Chernov, Y., Christensen, T.R., Huntley, B., Ims,  
653 R., Johansson, M., Jolly Riedlinger, D., Jonasson, S., Matveyeva, N., Oechel, W.,  
654 Panikov, N. and Shaver, G.: Arctic tundra and polar desert ecosystems, in: *Arctic Climate  
655 Impact Assessment*, edited by: ACIA, Cambridge University Press, 243–352, 2005.
- 656 Cannonea, N., Pontib, S., Christiansen, H.H., Christensen, T.R., Pirk, N. and Guglielmin, M.:  
657 Effects of active layer seasonal dynamics and plant phenology on CO<sub>2</sub> land atmosphere  
658 fluxes at polygonal tundra in the High Arctic, Svalbard, *Catena*, 174, 142–153,  
659 <https://doi.org/10.1016/j.catena.2018.11.013>, 2019.
- 660 Christensen, T.R., Johansson, T., Akerman, H.J. and Mastepanov, M.: Thawing sub-arctic  
661 permafrost: Effects on vegetation and methane emissions, *Geophysical Research Letters*,  
662 31, L04501, <https://doi.org/10.1029/2003GL018680>, 2004.
- 663 Christensen, T.R., Jackowicz-Korzynski, M., Aurela, M., Crill, P., Heliasz, M., Mastepanov, M.  
664 and Friberg, T.: Monitoring the Multi-Year Carbon Balance of a Subarctic Palsa Mire  
665 with Micrometeorological Techniques, *Ambio*, 41, 207–217,  
666 <https://doi.org/10.1007/s13280-012-0302-5>, 2012.
- 667 Euskirchen, E. S., Bret-Harte, M. S., Scott, G. J., Edgar, C., and Shaver, G. R.: Seasonal patterns  
668 of carbon dioxide and water fluxes in three representative tundra ecosystems in northern  
669 Alaska, *Ecosphere*, 3, 1–19, <https://doi.org/10.1890/ES11-00202.1>, 2012.
- 670  
671 Euskirchen, E.S., Bret-Harte, M.S., Shaver, G.R., Edgar, C.W., and Romanovsky, V.E.: Long-  
672 Term Release of Carbon Dioxide from Arctic Tundra Ecosystems in Alaska, *Ecosystems*,  
673 20, 960–974, <http://doi.org/10.1007/s10021-016-0085-9>, 2017.
- 674 Friedlingstein, P., Cox, P., Betts, R., Bopp, L., von Bloh, W., Brovkin, V., Cadule, P., Doney, S.,  
675 Eby, M., Fung, I., Bala, G., John, J., Jones, C., Joos, F., Kato, T., Kawamiya, M., Knorr,  
676 W., Lindsay, K., Matthews, H. D., Raddatz, T., Rayner, P., Reick, C., Roeckner, E.,  
677 Schnitzler, K. G., Schnur, R., Strassmann, K., Weaver, A. J., Yoshikawa, C., and Zeng,  
678 N.: Climate-carbon cycle feedback analysis: Results from the C4MIP model  
679 intercomparison, *J. Climate*, 19, 3337–3353, <https://doi.org/10.1175/JCLI3800.1>, 2006.
- 680 Friedlingstein, P., O’Sullivan, M., Jones, M.W. et al.: Global carbon budget 2010, *Earth Syst.  
681 Sci. Data*, 12, 3269–3340, <https://doi.org/10.5194/essd-12-3269-2020>, 2019.



- 682 Groendahl, L., Friborg, T., and Soegaard, H.: Temperature and snow-melt controls on  
683 interannual variability in carbon exchange in the high Arctic, *Theor. Appl. Climatol.*, 88,  
684 111–125, <http://doi.org/10.1007/s00704-005-0228-y>, 2007.
- 685 Hanssen-Bauer, I., Førlund, E.J., Hisdal, H., Mayer, S., Sandø, A.B. and Sorteberg, A.: Climate in  
686 Svalbard 2100 – a knowledge base for climate adaptation, Norwegian Environment  
687 Agency, Report no. 1/2019., 2019.
- 688 Hugelius, G., Strauss, J., Zubrzycki, S., Haren, J.W., Schuur, E.A.G., Ping, C.-L., Schirrmeister,  
689 L., Grosse, G., Michaelson, G.J., Koven, C.D., O'Donnell, J.A., Elberling, B., Mishra,  
690 U., Camill, P., Yu, Z., Palmtag, J. and Kuhry, P.: Estimated stocks of circumpolar  
691 permafrost carbon with quantified uncertainty ranges and identified data gaps,  
692 *Biogeosciences*, 11, 6573–6593, <http://doi.org/10.5194/bg-11-6573-2014>, 2014.
- 693 Jackowicz-Korczynski, M., Christensen, T. R., Backstrand, K., Crill, P., Friborg, T.,  
694 Mastepanov, M., and Strom, L.: Annual cycle of methane emission from a subarctic  
695 peatland, *J. Geophys. Res.-Biogeo.*, 115, G02009, <http://doi.org/10.1029/2008JG000913>,  
696 2010.
- 697 Kljun, N., Calanca, P., Rotach, M.W., and Schmid, H.P.: (2015). A simple two-dimensional  
698 parameterisation for Flux Footprint Prediction (FFP), *Geosci. Model Dev.*, 8, 3695-3713,  
699 <http://doi.or/10.5194/gmd-8-3695-2015>, 2015.
- 700 Li-Cor: EddyPro® Software (Version 6.0), Li-Cor Inc., Lincoln, USA, 2016.
- 701 Lloyd, J., and Taylor, J.A.: On the temperature dependence of soil respiration, *Functional*  
702 *Ecology*, 8(3), 315-323, 1994.
- 703 Lopez-Blanco, E., Lund, M., Williams, M., Tamstorf, M.P., Westergaard-Nielsen, A., Exbrayat,  
704 J.-F., Hansen, B.U., and Christensen, T.R.: Exchange of CO<sub>2</sub> in Arctic tundra: impacts of  
705 meteorological variations and biological disturbance, *Biogeosciences*, 14, 4467–4483,  
706 <https://doi.org/10.5194/bg-14-4467-2017>, 2017.
- 707 Lund, M., Falk, J. M., Friborg, T., Mbufong, H. N., Sigsgaard, C., Soegaard, H., and Tamstorf,  
708 M. P.: Trends in CO<sub>2</sub> exchange in a high Arctic tundra heath, 2000–2010, *J. Geophys.*  
709 *Res.- Biogeo.*, <https://doi.org/10.1029/2011JG001901>, 2012.
- 710 Lüers, J., Westermann, S., Piel, K., and Boike, J.: Annual CO<sub>2</sub> budget and seasonal CO<sub>2</sub>  
711 exchange signals at a high Arctic permafrost site on Spitsbergen, Svalbard archipelago,  
712 *Biogeosciences*, 11, 6307–6322, <http://doi.org/10.5194/bg-11-6307>, 2014.
- 713 Mastepanov, M., Sigsgaard, C., Dlugokencky, E. J., Houweling, S., Strom L., Tamstorf, M. P.,  
714 and Christensen, T. R.: Large tundra methane burst during onset of freezing, *Nature*, 456,  
715 628–631, <http://doi.org/10.1038/nature07464>, 2008.





- 716 Mastepanov, M., Sigsgaard, C., Tagesson, T., Ström, L., Tamstorf, M. P., Lund, M., and  
717 Christensen, T. R.: Revisiting factors controlling methane emissions from high-Arctic  
718 tundra, *Biogeosciences*, 10, 5139–5158, <https://doi.org/10.5194/bg-10-5139-2013>, 2013.
- 719 McGuire, A. D., Christensen, T. R., Hayes, D., Heroult, A., Euskirchen, E., Kimball, J. S.,  
720 Koven, C., Lafleur, P., Miller, P. A., Oechel, W., Peylin, P., Williams, M., and Yi, Y.: An  
721 assessment of the carbon balance of Arctic tundra: comparisons among observations,  
722 process models, and atmospheric inversions, *Biogeosciences*, 9, 3185–3204,  
723 <https://doi.org/10.5194/bg-9-3185-2012>, 2012.
- 724 Myers-Smith, I. H., Kerby, J. T., Phoenix, G. K., Bjerke, J. W., Epstein, H. E., Assman, J. J.,  
725 John, C., Adreu-Hayles, L., Angers-Blondin, S., Beck, P. S. A., Berner, L. T., Bhatt, U.  
726 S., Bjorkman, A. D., Blok, D., Bryn, A., Christiansen, C. T., Cornelissen, J. H. C.,  
727 Cunliffe, A. M., Elmendorf, S. C., Forbes, B. C., Goetz, S. J., Hollister, R. D., de Jong,  
728 R., Lorant, M. M., Marcias-Fauria, K., Maseyk, K., Normand, S., Olofsson, J., Parker,  
729 T. C., Parmentier, F.-J. W., Post, E., Schaepman-Strub, G., Stordal, F., Sullivan, P. F.,  
730 Thomas, H. J. D., Tømmervik, H., Treharne, R., Tweedie, C. E., Walker, D. A.,  
731 Wilmking, M. and Wipf, S.: Complexity revealed in the greening of the Arctic, *Nat.*  
732 *Clim. Chang.*, 10, 106–117, <https://doi.org/10.1038/s41558-019-0688>, 2020.
- 733 Oechel, W. C., C. A. Laskowski, G. Burba, B. Gioli, and Kalhori, A.A.M.: Annual patterns and  
734 budget of CO<sub>2</sub> flux in an Arctic tussock tundra ecosystem, *J. Geophys. Res. Biogeosci.*,  
735 119, 323–339, <http://doi.org/10.1002/2013JG002431>, 2014.
- 736 Pastorello, G., Trotta, C., Canfora, E. et al.: The FLUXNET2015 dataset and the ONEFlux  
737 processing pipeline for eddy covariance data, *Sci Data*, 7, 225,  
738 <https://doi.org/10.1038/s41597-020-0534-3>, 2020.
- 739 Pirk, N., Sievers, J., Mertes, J., Parmentier, F.-J. W., Mastepanov, M., and Christensen, T. R.:  
740 Spatial variability of CO<sub>2</sub> uptake in polygonal tundra: assessing low-frequency  
741 disturbances in eddy covariance flux estimates, *Biogeosciences*, 14, 3157–3169,  
742 <https://doi.org/10.5194/bg-14-3157-2017>, 2017.
- 743 Post, E., Forchhammer, M. C., Bret-Harte, M. S., Callaghan, T. V., Christensen, T. R., Elberling,  
744 B., Fox, A. D., Gilg, O., Hik, D. S., Høye, T. T., Ims, R. A., Jeppesen, E., Klein, D. R.,  
745 Madsen, J., McGuire, A. D., Rysgaard, S., Schindler, D. E., Stirling, I., Tamstorf, M. P.,  
746 Tyler, N. J. C., van der Wal, R., Welker, J., Wookey, P. A., Schmidt, M. and Astrup, P.:  
747 Ecological dynamics across the arctic associated with recent climate change, *Science*,  
748 325, 1355–1358, <http://doi.org/10.1126/science.117311>, 2009.
- 749 Ravolainen, V., Soininen, E. M., Jónsdóttir, I. S., Eischeid, I., Forchhammer, M., van der Wal,  
750 R. and Pedersen, A. Ø.: High Arctic ecosystem states: Conceptual models of vegetation  
751 change to guide long-term monitoring and research, *Ambio*, 49, 666–677,  
752 <https://doi.org/10.1007/s13280-019-01310-x>, 2020.



- 753 Rennermalm, A.K., Soegaard, H., and Nordstroem, C.: Interannual Variability in Carbon  
754 Dioxide Exchange from a High Arctic Fen Estimated by Measurements and Modeling,  
755 Arctic, Antarctic, and Alpine Research, 37(4), 545-556, [https://doi.org/10.1657/1523-0430\(2005\)037\[0545:IVICDE\]2.0.CO;2](https://doi.org/10.1657/1523-0430(2005)037[0545:IVICDE]2.0.CO;2), 2005.
- 757 Richardson, A. D., Braswell, B. H., Hollinger, D. Y., Jenkins, J. P. and Ollinger, S. V.: Near-  
758 surface remote sensing of spatial and temporal variation in canopy phenology, *Ecological*  
759 *Applications*, 19, 1417–1428, <http://doi.org/10.1890/08-2022.1>, 2009.
- 760 Sachs, T., Wille, C., Boike, J., and Kutzbach, L.: Environmental controls on ecosystem-scale  
761 CH<sub>4</sub> emission from polygonal tundra in the Lena river delta, Siberia, *J. Geophys. Res.-*  
762 *Biogeosci.*, 113, G00A03, <http://doi.org/10.1029/2007JG000505>, 2008.
- 763 Saunois, M., Stavert, A.R., Poulter, B et al.: The global methane budget 2000-2017, *Earth Syst.*  
764 *Sci. Data*, 12, 1561–1623, <https://doi.org/10.5194/essd-12-1561>, 2020.
- 765 Schimel, J.P.: Plant Transport and Methane Production as Controls on Methane Flux from Arctic  
766 Wet Meadow Tundra, *Biogeochemistry*, 28 (3), 183-200,  
767 <https://doi.org/10.1007/BF02186458>, 1995.
- 768 Schuur, E. A. G., McGuire, A. D., Schadel, C., Grosse, G., Harden, J. W., Hayes, D. J.,  
769 Hugelius, G., Koven, C. D., Kuhry, P., Lawrence, D. M., Natali, S. M., Olefeldt, D.,  
770 Romanovsky, V. E., Schaefer, K., Turetsky, M. R., Treat, C. C., and Vonk, J. E.: Climate  
771 change and the permafrost carbon feedback, *Nature*, 520, 171–179,  
772 <https://doi.org/10.1038/nature14338>, 2015.
- 773 Soegaard, H. & Nordstroem, C.: Carbon dioxide exchange in a high-arctic fen estimated by eddy  
774 covariance measurements and modeling, *Glob. Change Biol.*, 5, 547–562,  
775 <https://doi.org/10.1111/j.1365-2486.1999.00250.x>, 1999.
- 776 Strom, L., Tagesson, T., Mastepanov, M., and Christensen, T. R.: Presence of *Eriophorum*  
777 *scheuchzeri* enhances substrate availability and methane emission in an Arctic wetland,  
778 *Soil Biol. Biochem.*, 45, 61–70, <http://doi.org/10.1016/j.soilbio.2011.09.005>, 2012.
- 779  
780 Walker, D. A., Raynolds, M. K., Daniëls, F. J. A., Einarsson, E., Elvebakk, A., Gould, W. A.,  
781 Katenin, A. E., Kholod, S. S., Markon, C. J., Melnikov, E. S., Moskalenko, N. G., Talbot,  
782 S. S., Yurtsev, B. A. and the other members of the CAVM Team: The Circumpolar  
783 Arctic vegetation map, *Journal of Vegetation Science*, 16, 267-282,  
784 <https://doi.org/10.1111/j.1654-1103.2005.tb02365.x>, 2005.
- 785  
786 Vanderpuyse, A. W., Elvebakk, A. and Nilsen, L.: Plant communities along environmental  
787 gradients of high-arctic mires in Sassendalen, Svalbard, *J. Veg. Sci.*, 13, 875–884,  
788 <http://doi.org/10.1111/j.1654-1103.2002.tb02117.x>, 2002.
- 789



- 790 Wutzler, T., Lucas-Moffat, A., Migliavacca, M., Knauer, J., Sickel, K., Šigut, L., Menzer, O. and  
791 Reichstein, M.: Basic and extensible post-processing of eddy covariance flux data with  
792 REddyProc, *Biogeosciences*, 15(16), 5015-5030, Doi:10.5194/bg-15-5015-2018, 2018.
- 793 Zhang, W., Jansson, P-E., Sigsgaard, C., McConnella, A., Jammet, M.M., Westergaard-Nielsen,  
794 A., Lund, M., Friborg, T., Michelsen, A., and Elberling, B.: Model-data fusion to assess  
795 year-round CO<sub>2</sub> fluxes for an arctic heath ecosystem in West Greenland (69°N),  
796 *Agricultural and Forest Meteorology*, 272-273, 176-186,  
797 <https://doi.org/10.1016/j.agrformet.2019.02.021>, 2019.